Infrared and Raman spectra of silica polymorphs from an *ab initio* parametrized polarizable force field

Yunfeng Liang
International School for Advanced Studies (SISSA), Via Beirut 2-4, 34014 Trieste, Italy and INFM/Democritos, National Simulation Center, 34014 Trieste, Italy

Caetano R. Miranda and Sandro Scandolo[a)]
The Abdus Salam International Centre for Theoretical Physics (ICTP), Strada Costiera 11, 34014 Trieste, Italy and INFM/Democritos, National Simulation Center, 34014 Trieste, Italy

(Received 20 September 2006; accepted 17 October 2006; published online 21 November 2006)

The general aim of this study is to test the reliability of polarizable model potentials for the prediction of vibrational (infrared and Raman) spectra in highly anharmonic systems such as high temperature crystalline phases. By using an *ab initio* parametrized interatomic potential for SiO_2 and molecular dynamics simulations, we calculate the infrared and Raman spectra for quartz, cristobalite, and stishovite at various thermodynamic conditions. The model is found to perform very well in the prediction of infrared spectra. Raman peak positions are also reproduced very well by the model; however, Raman intensities calculated by explicitly taking the derivative of the polarizability with respect to the atomic displacements are found to be in poorer agreement than intensities calculated using a parametrized "bond polarizability" model. Calculated spectra for the high temperature β phases, where the role of dynamical disorder and anharmonicities is predominant, are found to be in excellent agreement with experiments. For the octahedral phases, our simulations are able to reproduce changes in the Raman spectra across the rutile-to-$CaCl_2$ transition around 50 GPa, including the observed phonon softening. © *2006 American Institute of Physics*. [DOI: 10.1063/1.2390709]

I. INTRODUCTION

Raman and infrared spectroscopies are routinely used as an experimental tool for the characterization of materials. By probing the vibrational dynamics of a material, they are very effective in providing information about its mechanical and elastic properties, as well as on the occurrence of structural phase transitions. In high-pressure physics, where alternative techniques are difficult to use in conjunction with diamond anvil cells, vibrational spectroscopies are instrumental to detect phase transitions. The theoretical determination of Raman and infrared (IR) spectra is a powerful complementary tool to experimental analysis, particularly at extreme conditions of pressure and temperature, where experiments are challenging. The theoretical analysis establishes a direct link between the peaks observed in the experimental spectra and the character of the underlying atomic dynamics and structure and can be used to validate or dismiss structural models. Theoretical efforts to model the vibrational dynamics of solids have been to a large extent limited to the harmonic approximation, whereby the vibrational density of states (VDOS) is obtained by direct diagonalization of the dynamical matrix obtained in the limit of small-amplitude harmonic oscillations of the atoms around their equilibrium positions. Theoretical models of IR and Raman spectra require, in addition to the VDOS, the calculation of the derivative of the polarization vector and of the polarizability tensor with respect to atomic displacements, respectively. The derivatives can either be obtained from simple empirical models or from an *ab initio* quantum treatment of the electronic response.[1–4] The harmonic approximation holds well for most solids at low temperatures. However, a large number of materials, including ferroelectrics, ionic conductors, and silicates, undergo phase transitions between ordered and disordered states (which are completely anharmonic) due to temperature and/or pressure changes. In addition, Raman spectra in various melts, especially, the liquid silicates in magmas, still lack a theoretical interpretation.[5–7] The harmonic approximation is obviously unable to describe such strongly anharmonic or fluid phases.

Attempts to go beyond the harmonic approximation normally range from the systematic calculation of higher-order contributions in terms of the atomic displacements from equilibrium to the full time-dependent treatment of the atomic trajectories by means of molecular dynamics (MD), the latter being applicable also to fluids, where atomic displacements from the initial positions can be arbitrarily large and power expansions ill defined. Within a molecular dynamics approach, the full VDOS can be calculated as the Fourier transform of the velocity-velocity autocorrelation function, and derivatives of the polarization and of the polarizability can be obtained "on the fly" at each instantaneous configuration of the system during its time evolution.[8] While this approach guarantees in principle a full treatment of the dynamics in anharmonic solids and in fluids and can be extended to include an *ab initio* calculation of the electronic

[a)]Electronic mail: scandolo@ictp.it

polarization and polarizability, a full quantum mechanical approach to the determination of Raman and IR spectra has so far been severely limited by the computational overhead of the quantum mechanical response and has been reported so far only for very simple systems.[9,10] In this context, it is clear that the development of simplified models for the calculation of Raman and IR spectra, which retain the accuracy of *ab initio* treatments but at a much reduced computational cost, would be extremely useful.

In this paper we present a model, based on molecular dynamics and on polarizable force field parametrized on *ab initio* calculations, which is able to reproduce the experimental spectra of various silica (SiO_2) polymorphs with good accuracy. The choice of silica was motivated by the availability of a polarizable force field from previous work and also by the need to test the method on a large variety of phases with different degrees of anharmonicity and/or dynamical disorder.

Silica exists in many different polymorphs, α- and β-quartz, α- and β-cristobalite, coesite, stishovite, and a $CaCl_2$-like form, each one thermodynamically stable in a different region of the phase diagram. Such a variety of phases offers an interesting stage for theoretical models. The most stable phase of silica at ambient condition is α-quartz, which belongs to the class of silica structures with corner-sharing SiO_4 tetrahedral. Quartz is traditionally considered a nontrivial benchmark system for examining the accuracy of the theory.[2,3] Cristobalite belongs to the same class of structures but has smaller density, different symmetry, and a different medium-and long-range arrangement of the tetrahedral. Besides their obvious relevance *per se*, understanding the Raman and IR spectra of both quartz and cristobalite might set a basis for the interpretation of vibrational spectra in silica glass, the disordered counterpart of the class of corner-sharing tetrahedral networks. By increasing temperature, quartz and cristobalite transform from a low temperature α phase, where the harmonic approximation is believed to be valid, into a β phase, whose dynamics is believed to be dominated by dynamical disorder and hence to be completely anharmonic. Raman and IR experiments on quartz and cristobalite as a function of temperature show that the α-β transition is characterized by the sudden disappearance, in the high temperature β phases, of some of the peaks of the low temperature α phases.[11–14] In quartz, the Raman modes present at 128 and 207 cm^{-1} in the α phase merge and weaken, and only one major peak remains in the spectrum of β-quartz around 464 cm^{-1}, slightly left shifted with respect to the same peak in α-quartz.[12] For cristobalite, all the strong Raman bands at 416, 230, and 114 cm^{-1} disappear in the transition of α-cristobalite to β-cristobalite.[13,14] Stishovite (rutile structure) and the $CaCl_2$-like phase of silica are also of considerable interest not only because of their edge-sharing SiO_6 octahedral structures, with Si in sixfold coordination to O, but also because the pressure-induced rutile-to-$CaCl_2$ transition is a typical example of a soft-mode-induced Laudau-type transition, as first found by Raman spectroscopy[15] and later confirmed by x-ray diffraction.[16]

Calculating infrared spectra from model potentials requires the knowledge of the polarization changes during the dynamics, which can be extracted from classical[17–20] or from *ab initio* simulations.[10] The results in the case of classical simulations depend on the potential employed, so the ability of a potential to reproduce infrared spectra has become an important criterion in determining the quality of a potential and in identifying the relevant interactions.[17–20] For example, the most widely used force fields for silica, such as the TTAM (Ref. 21) and BKS (Ref. 22) potentials, showed some difficulties in reproducing the infrared spectra of silica polymorphs.[18,19] Calculating Raman spectra requires, in addition to the polarization, also the knowledge of the electronic linear response to an electric field (i.e., the polarizability) of the system during the vibrational dynamics. *Ab initio* approaches can provide such a response, albeit with a substantial computational effort. On the other hand, empirical approaches based on rigid charges, such as the TTAM and BKS potentials, are unable, by construction, to simulate the electronic response, which explains why no attempt has been made so far to provide a theoretical model for the vibrational spectra of the high temperature β phases. We have recently developed a new polarizable force field for silica (the TS potential[23]), which describes experimental data on the structural properties of most SiO_2 low-pressure crystalline polymorphs, liquid and glass, better than any other empirical model,[23–25] as detailed in Sec. II A. For the purpose of the present paper, however, the main advantage of the TS potential, with respect to rigid-ion models, is its fluctuating-dipole feature, which implies that the polarizability of the system (and thus its Raman spectra) can be extracted from the model itself, without further empirical and/or external assumptions. The reliability of the Raman spectra calculated with the TS potential is not obvious *a priori*, as the parameters of the potential were fitted to reproduce *ab initio* forces, stresses, and energies on selected configurations, while the electronic response was not included explicitly in the set of physical quantities to which the potential was fitted. So the possibility exists that the parameters related to the induced fluctuating dipoles took effective values able to reproduce the structural properties, but perhaps not the electronic response, as recently shown in the case of the piezoelectrical constant.[26]

The goal of this work is twofold. On one hand we determine the accuracy of the TS potential in reproducing the Raman and IR spectra of selected silica polymorphs, including octahedral phases. On the other hand, we present a model, based on molecular dynamics, which is capable of simulating Raman and IR spectra at arbitrary temperatures, up to the fully anharmonic regime. The paper is organized as follows: in Sec. II we give a brief overview of the calculation methods. In Sec. III we present the infrared spectra for the low-pressure phases (quartz and cristobalite) and the high-pressure phase stishovite and compare them with the results of other potentials. In Sec. IV A, we present Raman spectra for quartz and cristobalite at low temperatures and discuss the reliability of the Raman spectra calculated with the TS potential. In Sec. IV B, we present Raman spectra for quartz and cristobalite at high temperatures. In Sec. IV C we de-

scribe the Raman spectra of stishovite and how it changes across the rutile-to-$CaCl_2$ transition. We summarize our results in Sec. V.

II. COMPUTATIONAL METHODS

A. The potential

In the present work, the TS potential[23] is employed to model α- and β-quartz, α- and β-cristobalite, stishovite, and a $CaCl_2$-like phase. The quest for a better potential for silica polymorphs has a long history, which started with the observation that an effective empirical pair potential could describe the relevant structural and dynamical features of silica liquid and glass.[27] Explicit inclusion of covalency in Si–O bonds was achieved by adding three-body contributions.[28,17] The TTAM pair potential[21] was regarded as an important development, because its parameters were fitted to *ab initio* data (on small clusters) and because partial covalence was modeled by the use of partial charges and a compensating short-range attraction. The BKS potential[22] went further along this line by reparametrizing the TTAM potential on experimental data for quartz, an extended solid. The deficiencies of rigid-ion models have been neatly discussed by Wilson *et al.*[20] In particular, rigid-ion models were shown to be unable to reproduce the experimental gap between stretching and bending frequencies in the infrared spectra of silica glass. It was instead shown that by allowing oxygen ions to be polarizable, the infrared spectra could be substantially improved. The TS potential was developed starting from the ideas of Wilson *et al.* with the additional feature that its parameters were obtained by best fit to forces, stresses, and energies obtained by *ab initio* methods on selected configurations in the liquid.[23] Previous simulations using the TS potential are in very good agreement with experimental data on the structural properties of most SiO_2 low-pressure crystalline polymorphs, liquid and glass.[23–25] The temperature dependence of the c/a ratio in α- and β-quartz (Fig. 4 in Ref. 24) and pressure dependence of the lattice constant across the rutile-to-$CaCl_2$ transition (Fig. 14 in Ref. 24) are just a few examples of the accuracy of the potential with respect to other existing force fields for silica. The TS potential has been shown to reproduce the Si–O–Si angular distribution in the liquid and in all the low-pressure crystalline silica phases better than rigid-ion potentials.[23] The Si–O–Si angle distribution is believed to be tightly correlated with Raman spectra.[2,29–31] Recent work has shown that the TS potential agrees very well with *ab initio* calculations on the VDOS of quartz,[24] indicating that the vibrational properties are also reproduced faithfully by the TS potential.

B. Infrared and Raman spectra

The infrared spectra have been calculated from the Fourier transform of the total polarization autocorrelation function, as already done for other potentials:[17–20]

$$I(\omega) = \frac{4\pi^2\omega}{3hcn}(1-\exp(-h\omega/K_BT)) \times \int_{-\infty}^{\infty} dt e^{-i\omega t}\langle \mathbf{P}(t)\cdot\mathbf{P}(0)\rangle, \quad (1)$$

where n is the refractive index of the medium, which for practical purposes can be treated as a constant in the calculation, h is the Planck constant, c is the speed of light, K_B is the Boltzmann constant, T is the temperature, $\mathbf{P}(t)$ is the total polarization vector at time t, which includes rigid charges and induced and short-range dipoles,[23] and angular brackets indicate the statistical average.

Raman spectra reported in this work have been calculated by Fourier transforming the dynamical autocorrelation functions of the electronic contribution to the polarizability tensor $\boldsymbol{\alpha}$.[8,9] Following the procedure in Ref. 9, we divide $\boldsymbol{\alpha}$ into its scalar part α and anisotropic part $\boldsymbol{\beta}$ so that

$$\boldsymbol{\alpha}(t) = \alpha(t)I + \boldsymbol{\beta}(t), \quad (2)$$

where $\alpha(t)=\frac{1}{3}\mathrm{Tr}\,\boldsymbol{\alpha}(t)$ and I is the identity matrix. Then it can be shown that the polarized component of Raman intensity is given by

$$I_{VV}(\omega) = I_{\mathrm{ISO}}(\omega) + \tfrac{4}{3}I_{VH}(\omega), \quad (3)$$

where ω is the frequency of the Raman spectra, with the isotropic scattering component given by

$$I_{\mathrm{ISO}}(\omega) = \frac{1}{2\pi}\int dt e^{-i\omega t}\langle\alpha(0)\alpha(t)\rangle \quad (4)$$

and the depolarized (or anisotropic) component by

$$I_{VH}(\omega) = \frac{1}{2\pi}\int dt e^{-i\omega t}\frac{1}{10}\langle \mathrm{Tr}[\overleftrightarrow{\beta}(0)\cdot\overleftrightarrow{\beta}(t)]\rangle. \quad (5)$$

Because the correlation functions are computed classically, quantum effect corrections[9] are taken into account by multiplying Eqs. (4) and (5) by a factor of $[1-e^{(-h\omega/KT)}/2]$.

We calculated the tensor $\boldsymbol{\alpha}$ with two different approaches. In the "direct" approach, $\boldsymbol{\alpha}$ was calculated as the derivative of the instantaneous electronic polarization with respect to an external electric field. The polarizability tensor was also calculated at each step using the bond polarizability model,[3] as discussed below.

C. The direct approach

In the direct approach, $\boldsymbol{\alpha}$ was calculated as

$$\alpha_{\mu\nu} = -\frac{\partial P_\mu}{\partial E_\nu}, \quad (6)$$

where $\mathbf{P}$ is the polarization vector, $\mathbf{E}$ is the applied electric field, and μ and ν are x, y, z in Cartesian coordinates. The derivative on (6) was calculated by finite differences at each MD step, by keeping atoms fixed. We found that $E=0.001$ a.u. guarantees that we are still in the linear regime, with negligible numerical noise. As a test of the accuracy of the method, we computed the electronic contribution (ε^∞) to the dielectric tensor of α-quartz as $\varepsilon^\infty_{\mu\nu}=\delta_{\mu\nu}+4\pi\langle\alpha_{\mu\nu}\rangle$, where the average is taken over a MD trajectory at 0 GPa and

300 K. We obtained similar values for the parallel ($\varepsilon_{\parallel}=2.295$) and perpendicular ($\varepsilon_{\perp}=2.290$) directions to the optical axis (z axis), which are in excellent agreement with the experiments ($\varepsilon_{\parallel}=2.383$ and $\varepsilon_{\perp}=2.356$).[32]

D. The bond polarizability model

The polarizability tensor $\boldsymbol{\alpha}$ was also calculated, at each MD step, with the so-called bond polarizability model (BP model),[3] in which the polarizability is parametrized in terms of bond contributions as follows:

$$\alpha_{\mu\nu}=\frac{1}{3}(2\alpha_p+\alpha_l)\delta_{\mu\nu}+(\alpha_l-\alpha_p)\left(\frac{R_\mu R_\nu}{|\mathbf{R}|^2}-\frac{1}{3}\delta_{\mu\nu}\right), \quad (7)$$

where $\mathbf{R}=\mathbf{R}_O-\mathbf{R}_{Si}$ is the vector connecting a bonded pair of oxygen and silicon atoms located at $\mathbf{R}_O$ and $\mathbf{R}_{Si}$, respectively. The parameters α_l and α_p define the longitudinal and perpendicular contributions to the bond polarizability, respectively, and depend on the length of the Si–O bond with the following derivative:

$$\frac{\partial\alpha_{\mu\nu}}{\partial R_\kappa}=\frac{1}{3}(2\alpha_p'+\alpha_l')\delta_{\mu\nu}\hat{R}_\kappa+(\alpha_l'-\alpha_p')\left(\hat{R}_\mu\hat{R}_\nu-\frac{1}{3}\delta_{\mu\nu}\right)\hat{R}_\kappa + \frac{(\alpha_l-\alpha_p)}{|\mathbf{R}|}(\delta_{\mu\kappa}\hat{R}_\nu+\delta_{\nu\kappa}\hat{R}_\mu-2\hat{R}_\mu\hat{R}_\nu\hat{R}_\kappa), \quad (8)$$

where $\hat{R}$ is a unit vector along $\mathbf{R}$ and α_l' and α_p' are the derivatives of the bond polarizabilities with respect to the bond length. Notice that only the derivative of the bond polarizability is needed, as only its time-dependent changes, and not its absolute values, enter in the construction of the Raman intensity. The derivative of the polarizability is thus completely defined in the BP model by three parameters:

$$\alpha=2\alpha_p'+\alpha_l', \quad \beta=\alpha_l'-\alpha_p', \quad \gamma=\frac{\alpha_l-\alpha_p}{R}. \quad (9)$$

Here we used the parameters of Ref. 3, which were determined by *ab initio* density functional methods. In order to calculate Raman intensities with the BP model we generated a MD trajectory with the TS potential and extracted the fluctuating part of the bond lengths by substracting from their instantaneous values the average value of the individual Si–O bonds averaged along the full trajectory. The total polarizability at each MD time step was finally determined by means of Eq. (6), by summing over all the Si–O bonds.

We will use both the direct method and the BP model to construct the polarizability of α-cristobalite and quartz. For the octahedral phases, however, no bond polarizability model exists to our knowledge, so the polarizability was determined exclusively using the direct method. It is important to remark that while the BP model has been widely employed so far to construct Raman spectra for silica polymorphs,[33] most of the calculations reported in the literature so far have been obtained in the harmonic approximation, and no calculation has been thus reported for high temperature β phases.

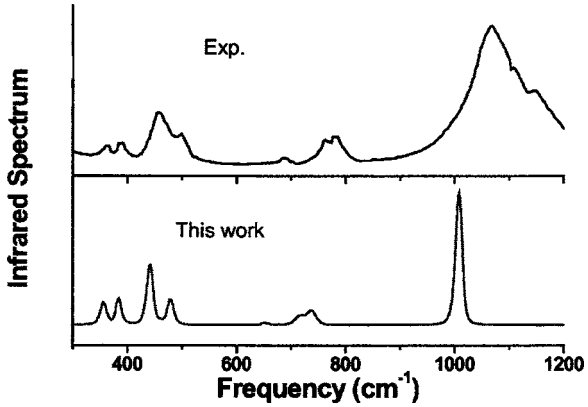

FIG. 1. Infrared spectra for α-quartz at 0 GPa and 300 K. The upper panel is experiments (Ref. 35); the lower panel is our calculation.

E. Details of the molecular dynamics

The MD trajectories were obtained in the microcanonical (*NVE*) ensemble. For quartz we used a simulation cell containing $2\times2\times2$ α-quartz unit cells (for a total of 24 SiO_2 units), for cristobalite a cell with $2\times2\times2$ α-cristobalite unit cells (32 SiO_2 units), and for stishovite a cell with $2\times2\times4$ stishovite unit cells (32 SiO_2 units). The Verlet algorithm was used to integrate Newton's equations of motion and the time step was set to 0.723 fs throughout this work. The initial atomic configurations at low temperature were taken from the ideal crystal structures,[34] and the initial velocities were taken from a Gaussian random distribution. Simulations of the high temperature and high-pressure phases were either started from the structures of Ref. 24 or obtained with the TS potential in the *NPT* ensemble by increasing temperature/or pressure very slowly. Equilibration times were of the order of 200 ps for the *NPT* runs, which were followed by about 200 ps in the *NVT* ensemble. Finally, runs longer than 200 ps were performed in the microcanonical ensemble to construct the correlation functions. The finite length of the runs introduces a 2–3 cm^{-1} broadening in the spectra, which was convoluted with an additional empirical broadening of 4 cm^{-1}.

III. INFRARED SPECTRA

In this section we compare infrared spectra for quartz, cristobalite, and stishovite with experiments, as well as with spectra obtained with other force fields, such as TTAM,[21] BKS,[22] and three-body potentials.[17] Infrared spectra for low-pressure and low temperature crystalline phases, α-quartz and cristobalite, are in excellent agreement with experimental data,[35,11] as shown in Figs. 1 and 2, respectively. Calculated frequencies are systematically underestimated, but differences are below 7%–8%. Intensities are also in fair agreement with experiments, if one considers that experimental spectra are obtained from powders and are generally broad, as a consequence of grain shape heterogeneity.[35] A comparison with the infrared spectra obtained with the BKS potential[18] shows that the addition of polarization effects can greatly improve the quality of simulated infrared spectra, particularly for what concerns intensities, as already noted for silica glass by Wilson *et al.*[20]

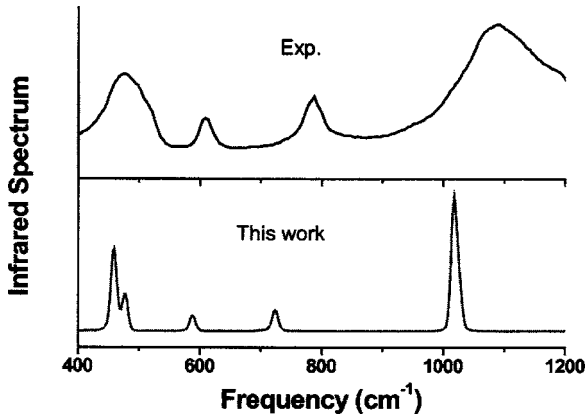

FIG. 2. Infrared spectra for α-cristobalite at 0 GPa and 100 K. The upper panel is experiments (Ref. 11); the lower panel is our calculations.

Comparison of our results for cristobalite with those obtained with a charge-transfer three-body potential[17] shows that the two models have similar intensity ratios and that both compare well with experiments. However, peak positions with the three-body potential are in worse agreement with experiments than those obtained with the TS potential. In addition, the α to β transition is estimated to take place around 1000 K with the three-body potential,[17] in contrast with experimental values ranging from 393 to 545 K,[36] while the TS potential gives a value within the experimental range.[24] In Fig. 3 we show the calculated infrared spectrum of high temperature β-cristobalite, together with the experimental data.[11] The peak at around 600 cm^{-1} in the α phase disappears in the β phase, in agreement with experiments and with the results obtained with the three-body potential.[17]

The TS potential employed in this work was obtained by best fit to *ab initio* data in liquid silica at low pressure, i.e., in a regime where the Si–O coordination is close to four, but for a few coordination defects. The applicability of the TS potential to sixfold coordinated, octahedral phases, such as stishovite, is thus not straightforward. However, the TS potential was recently shown to reproduce very well the c/a ratio[24] during the rutile-to-$CaCl_2$ transitions in stishovite. The lattice constants a and b predicted by the TS potential are also in excellent agreement with experiments and show a clear Landau-type transition around 50 GPa.[24] The only discrepancy with experiment is that the lattice constant is systematically overestimated in the simulation. While we believe that the problem might be solved by modifying the potential so as to allow the ion size and shape to vary, similarly to MgO,[37] we also believe that it is important to assess whether the accuracy of the potential in its present form can be extended to octahedral phases also for what concerns the Raman and IR spectra. We show in Fig. 4 the calculated IR spectra of stishovite at 9 GPa with experimental spectra obtained at ambient pressure,[38] since we could not stabilize stishovite at ambient pressure and no experimental spectra with intensities are available at finite pressure. The position of the peaks in the calculated spectra is in fair agreement with the position of the main experimental peaks.[38] Consistent with experiments, the peak corresponding to the octahedral Si–O stretching mode lies around 800 cm^{-1}. Our results are in much better agreement with experiments than those obtained with the BKS model,[18] where all peaks lie in the 500–620 cm^{-1} range, and those obtained with a charge-transfer three-body potential,[39] where only two peaks were reported around 800–1000 cm^{-1}.

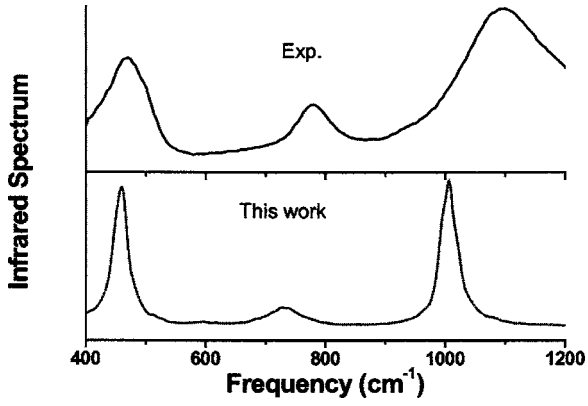

FIG. 3. Infrared spectra for β-cristobalite at 0 GPa and 600 K. The upper panel is experiments (Ref. 11); the lower panel is our calculations. Note the disappearance of the 590 cm^{-1} band [609 cm^{-1} in experiments (Ref. 11)] as a result of the α to β transition.

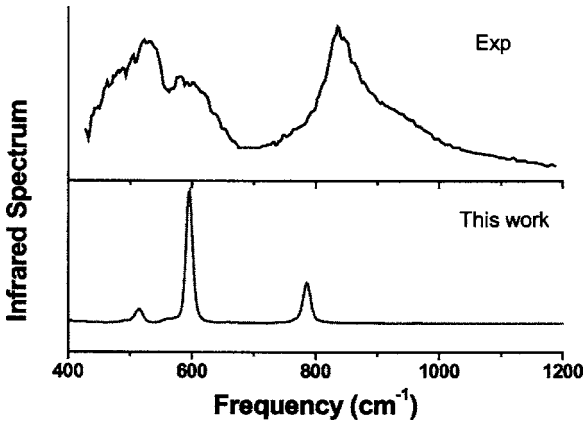

FIG. 4. Infrared spectra for stishovite at 9 GPa and 300 K. The upper panel is experiments at 1 atm and room temperature (see text for explanation)(Ref. 38); the lower panel is our calculations.

IV. RAMAN SPECTRA

A. Low temperature tetrahedral phases

We first compare the Raman spectra calculated using the BP model (Sec. II D) with experiments and *ab initio* calculations. Raman spectra for the low-pressure and low temperature crystalline phases, α-quartz and α-cristobalite, are presented in Figs. 5 and 6, respectively. The spectra are in excellent agreement with experimental data[12,13,29,40] and with *ab initio* calculations,[4] especially concerning the Raman peak positions. The three main peaks for α-quartz are found at 129, 205, and 467 cm^{-1} in our simulations, compared with 128, 207(6), and 464 cm^{-1} in experiments, respectively.[12,29] The two main peaks for α-cristobalite are at 223 and 409 cm^{-1} in our simulations, compared with 230 and 416 cm^{-1} in experiments.[13] A weaker peak at around 114 cm^{-1} for α-cristobalite is found both in *ab initio* and our calculations. Such accuracy in the peak positions is beyond

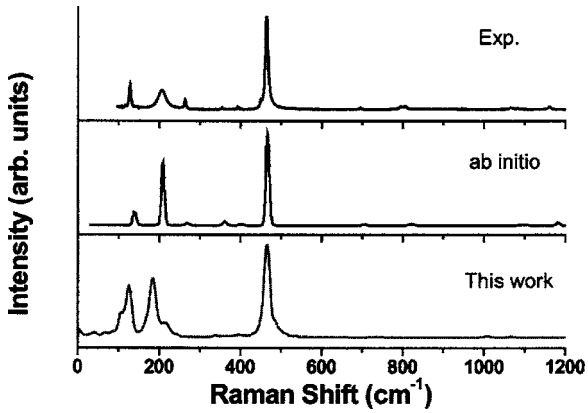

FIG. 5. Raman spectra for α-quartz at 0 GPa and 300 K. The top panel is experiments (Ref. 29); the middle panel is *ab initio* calculations (Ref. 4); the bottom panel is our calculations, based on the bond polarizability model (seen in Sec. II D) and the trajectory generated by MD simulations with the TS potential. Theoretical data are convoluted with a uniform Gaussian broadening with width σ=4 cm^{-1}.

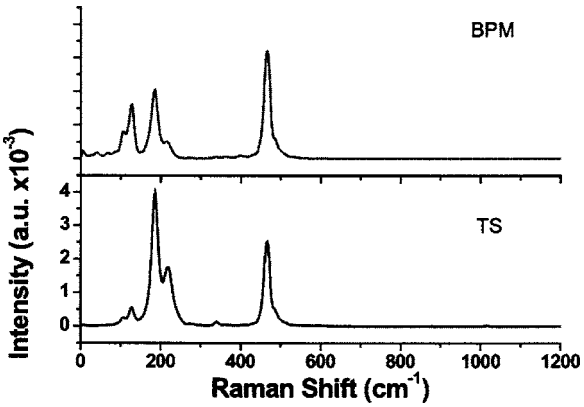

FIG. 7. Isotropic part of the Raman spectra for α-quartz at 300 K and 0 GPa. In the upper panel, the intensity is obtained by the BP model (see Sec. II D); in the lower panel it is obtained with the direct approach (see Sec. II C).

expectations and is probably due to a compensation of errors. The *ab initio* frequencies of Ref. 4, shown in Figs. 5 and 6, were in fact rescaled by 5% to match the experimental spectra. The TS potential was constructed to match the *ab initio* potential, so a similar error (5%) would be expected, with respect to experimental data, in case of perfect fit. Therefore, the accuracy of the TS results ($<$3%) must be the consequence of a compensation between the *ab initio* intrinsic error and the residual fit error.

Intensities calculated with the BP model are known to be accurate,[2,3] so the agreement between theoretical and experimental intensities in Figs. 5 and 6 is not surprising. Intensities calculated with the direct approach (Sec. II C) turn out to be in worse agreement with experiments than those obtained with the BP model. In Figs. 7–9, we compare isotropic and anisotropic parts [as defined in Eqs. (4) and (5)], calculated with the two approaches for α-quartz and α-cristobalite. The peak positions are obviously the same in the two approaches, as the same MD trajectory was employed. The intensities of the isotropic parts calculated with the two approaches are also in good agreement. However, regarding the anisotropic part, the direct approach seems to perform rather badly for what concerns intensities, which are about one order of magnitude larger than with the BP model. Because the spectra obtained with the BP model are in good agreement with experiment, we conclude that the current implementation of the polarizability in the TS model serves very well the purpose of providing accurate force on the atoms and first derivatives of the polarization (such as effective charges and dielectric constant) but needs further improvement in order to match the accuracy of the BP model in the calculation of higher-order derivatives such as Raman intensities. For this reason, Raman spectra for the tetrahedral phases at high temperature will be calculated using the BP model only.

B. High temperature tetrahedral phases

Raman spectra calculated using the BP model (Sec. II D) for the high temperature and low-pressure crystalline phases, β-quartz and cristobalite, are compared with experimental data[12,13] in Figs. 10 and 11, respectively. We find an excellent agreement with experiments in both cases. For quartz, the modes at 129 and 205 cm^{-1} merge and are drastically attenuated; the peak around 467 cm^{-1} in α-quartz is left shifted to 458 cm^{-1}, to be compared with a peak position at 459 cm^{-1} in experiments.[12] For cristobalite all major bands (at 110, 223, and 409 cm^{-1}) merge into a structureless bump, in agreement with experiments.[13,14] It is important to notice that Raman spectra at high temperature differ substantially with

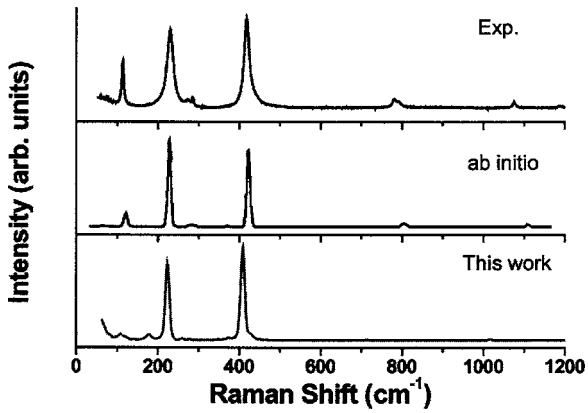

FIG. 6. Raman spectra for α-cristobalite at 0 GPa and 100 K. Panels are the same as in Fig. 5.

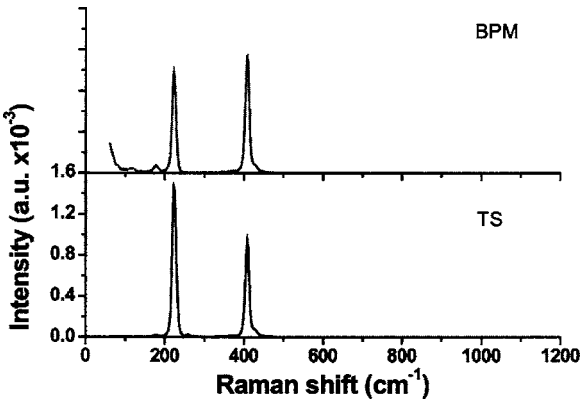

FIG. 8. Isotropic part of the Raman spectra for α-cristobalite at 100 K and 0 GPa. Panels are the same as in Fig. 7.

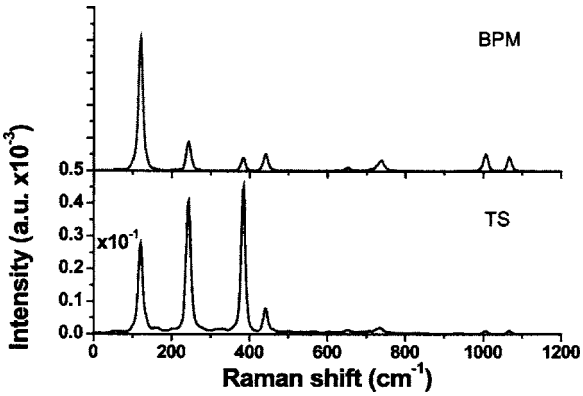

FIG. 9. Anisotropic part of the Raman spectra for α-quartz. Panels are the same as in Fig. 7.

respect to the low temperature phases. In cristobalite no clear peak is observed above the transition temperature, and in quartz only one sharp peak around 460 cm^{-1} remains. The capability of our theoretical approach to reproduce the changes in the experimental spectra across the α-β transition suggests that the method can be applied with confidence in the study of temperature-induced transitions where the role of dynamical disorder and anharmonicities is predominant. We also remark that this is the first theoretical attempt to model Raman spectra in high temperature silica phases.

The atomistic mechanisms of the α-β transformations and the nature of the high temperature phases are still a subject of debate,[14,41–48] and the correct interpretation of Raman and IR spectra may provide important hints to the solution of the debate. For example, the disappearance of the Raman and IR peaks in cristobalite has been used to rule out domain models of the transition.[14] The modes around 400–600 cm^{-1} are particularly interesting because they are connected with the displacement of oxygen atoms along the bisector direction of the Si–O–Si bond angle.[2,28–30] In the high temperature (β) phases, the Si–O–Si plane normal undergoes reversals, as

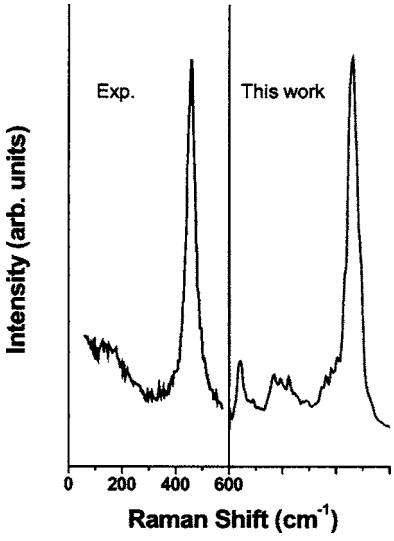

FIG. 10. Raman spectra for β-quartz at 0 GPa and 750 K. The left panel is experimental data from Ref. 12; the right panel is our calculations based on the BP model. The simulated data are convoluted with a uniform Gaussian broadening with width σ=4 cm^{-1} as in Fig. 5.

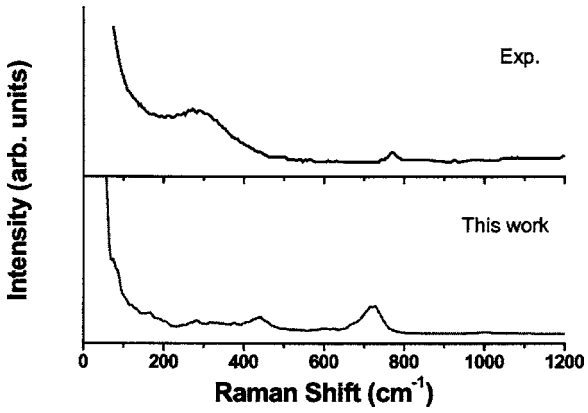

FIG. 11. Raman spectra for β-cristobalite at 0 GPa and 600 K. The upper panel is experimental data from Ref. 13; the bottom panel is our calculations based on the BP model.

shown by Huang and Kieffer.[17,41] In β-cristobalite, the distribution of the Si–O–Si plane normal is such that for any direction of the plane normal there is an equal probability of finding its opposite. Because in a simple bond polarization picture the plane reversals change the sign of their individual contributions to the total Raman signal, the Raman intensity around 400–600 cm^{-1} in β-cristobalite is very weak. On the contrary, in quartz, the α-β transition is characterized, on average, by a 45° flip of the Si–O–Si plane normal,[43] which breaks the "inversion" symmetry discussed above for β-cristobalite and preserves the finite intensity of this mode at around 460 cm^{-1}.

C. Octahedral phases

We focus here on the rutile-to-$CaCl_2$ transition reported to take place in experiments around 50 GPa. We notice that no BP model parameterization exists for octahedral silica, so we are forced to use the direct method (Sec. II C). In Fig. 12 we compare calculated and experimental Raman spectra for stishovite. Calculations were performed again at 9 GPa, as we could not stabilize stishovite at ambient pressure. No clean experimental spectra with intensities are available at finite pressure, so we report in Fig. 12 experimental spectra obtained at ambient pressure.[12,40,49] Pressure corrections in

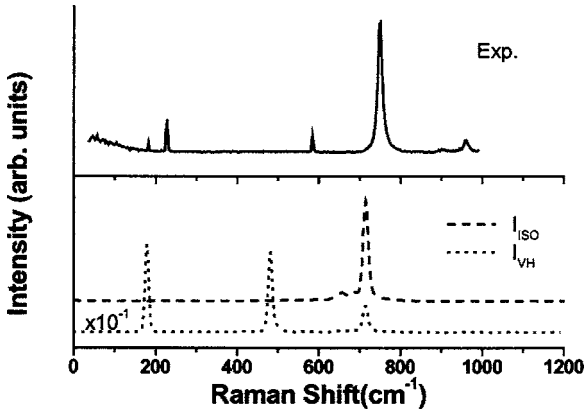

FIG. 12. Raman spectra for stishovite at 9 GPa and 300 K. The upper panel is experimental data at 1 atm from Ref. 12; the bottom panel is our calculations using the direct approach (see Sec. II C).

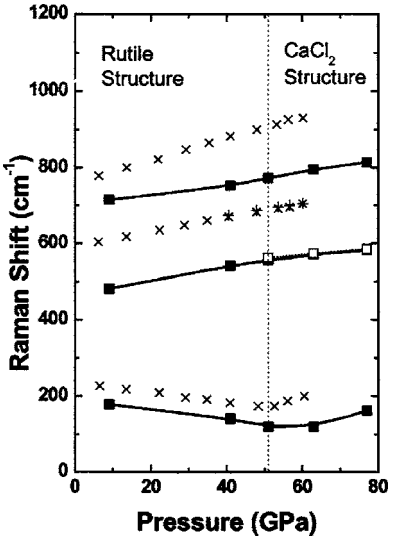

FIG. 13. Raman shifts with pressure during the rutile-to-$CaCl_2$ transition. Crosses are experimental data from Ref. 15; squares are our calculations; lines are guide for the eyes. The lowest frequency mode clearly shows a softening around 50 GPa.

the Raman peak positions amount to less than 30 cm^{-1} between 0 and 9 GPa.[15] The results are in qualitative agreement with the experimental spectra; however, the peak positions are systematically underestimated and, like in quartz, the intensity of the anisotropic part is overestimated. Nevertheless, it is instructive to notice that the peaks at 180 and 480 cm^{-1} only come from the anisotropic part.

The pressure-induced rutile-to-$CaCl_2$ transition is a typical example of a soft-mode-induced Laudau-type transition, as first found by Raman spectroscopy[15] and later confirmed by x-ray diffraction.[16] A detailed theoretical study of this subtle transition is potentially useful in the modeling of silica at high pressure. In Fig. 13 we show the pressure dependence of the vibrational modes for the stishovite and compare it with experiments.[15] In spite of the poor accuracy in the absolute positions of the peaks, their pressure dependence appears to be correctly captured by the model. In particular, the lowest peak shows a softening behavior below 51 GPa, which is consistent with experiments[15,50] and simulations.[15,51,52] Our simulations also reproduce the subsequent increase in the peak position after the transition. Considering that the TS potential was optimized for tetrahedral, low-pressure phases, the present results are quite encouraging and confirm that its range of applicability could be substantially larger and include octahedral phases, even though with a reduced accuracy.

V. CONCLUSIONS

By using an improved, *ab initio* parametrized interatomic potential for SiO_2, we first calculated infrared and Raman spectra for quartz, cristobalite, and stishovite and compared them with experiments, as well as with spectra obtained with other force fields, such as TTAM, BKS, and an improved three-body potential. The reliability of our interaction potential in the calculation of IR spectra is validated by the excellent agreement with experimental IR data both in the peak positions and in the relative intensities. In particular, we were able to reproduce the relevant spectral changes mode in the α-β transition of cristobalite. For the octahedral phases, even though the agreement with experiments is worse than for the low-pressure phases, the potential reproduces the three main modes with reasonable accuracy.

In the case of Raman spectra, peak positions turned out to be in good agreement with experimental and *ab initio* calculations. However, intensities determined by explicitly calculating the derivatives of the polarizability with respect to atomic displacements turned out to be in worse agreement with experiments than those obtained when a parametrized bond polarizability model was employed. Raman spectra calculated using the bond polarizability model for the high temperature and low-pressure crystalline phases, β-quartz and β-cristobalite, were found to be in excellent agreement with experiments. It is important to remark that the atomic dynamics in the proximity of α-β transitions and in the high temperature β phases are generally considered to be highly nonharmonic. Our results suggest that the present method can be extended to the study of other temperature-induced transitions where the role of dynamical disorder and anharmonicities is predominant. The performance of our potential in octahedral structures was evaluated by calculating Raman spectra across the rutile-to-$CaCl_2$ transition at around 50 GPa. In spite of the poor accuracy in the absolute positions of the peaks and the relative intensities, their pressure dependence appears to be correctly captured by the model. In particular, the lowest frequency peak shows a softening behavior below $\sim$50 GPa, which is consistent with experiments and other calculations.

Polarizable model potentials are increasingly used in the simulation of water and biomolecular systems,[53] where vibrational spectroscopy is still a primary source of information about microscopic structure and dynamics. Our study highlights virtues and deficiencies of a polarizable model in the determination of Raman and IR spectra in the highly anharmonic regime in the specific case of silica. The study shows that our silica model performs very well for IR spectra but suggests that improvements are required in the polarization part before a satisfactory agreement with experiments can be reached on Raman intensities. On the other hand, combining the MD trajectories obtained with our polarizable potential with a parametrized model for the polarizability yields results in very good agreement with experiments for Raman intensities.

ACKNOWLEDGMENTS

We thank M. Lazzeri and P. Tangney for useful discussions and acknowledge partial support from CNR through the ESF program "EuroMinSci."

[1] A. Pasquarello and R. Car, Phys. Rev. Lett. **79**, 1766 (1997).
[2] P. Umari, X. Gonze, and A. Pasquarello, Phys. Rev. Lett. **90**, 027401 (2003).
[3] P. Umari, A. Pasquarello, and A. Dal Corso, Phys. Rev. B **63**, 094305 (2001).
[4] M. Lazzeri and F. Mauri, Phys. Rev. Lett. **90**, 036401 (2003).
[5] P. F. Mcmillan, B. T. Poe, P. Gillet, and B. Reynard, Geochim. Cosmo-

chim. Acta **58**, 3653 (1994); P. Gillet, Phys. Chem. Miner. **23**, 263 (1996).
[6] A. G. Kalampounias, S. N. Yannopoulos, and G. N. Papatheodorou, J. Chem. Phys. **124**, 014504 (2006).
[7] Y. Q. Wu, G. C. Jiang, J. L. You, H. Y. Hou, H. Chen, and K. D. Xu, J. Chem. Phys. **121**, 7883 (2004).
[8] B. J. Berne and R. Pecora, *Dynamic Light Scattering* (Wiley, New York, 1976).
[9] A. Putrino and M. Parrinello, Phys. Rev. Lett. **88**, 176401 (2002).
[10] M. Sharma, R. Resta, and R. Car, Phys. Rev. Lett. **95**, 187401 (2005); M. Bernasconi, P. L. Silvestrelli, and M. Parrinello, *ibid.* **81**, 1235 (1998); P. L. Silvestrelli, M. Bernasconi, and M. Parrinello, Chem. Phys. Lett. **277**, 478 (1997); A. Debernardi, M. Bernasconi, M. Cardona, and M. Perrinello, Appl. Phys. Lett. **71**, 2692 (1997).
[11] K. S. Finnie, J. G. Thompson, and R. L. Withers, J. Phys. Chem. Solids **55**, 23 (1994).
[12] P. Gillet, A. Le Cleach, and M. Madon, J. Geophys. Res. **95**, 21635 (1990).
[13] J. Bates, J. Chem. Phys. **57**, 4042 (1972).
[14] I. P. Swainson, M. T. Dove, and D. C. Palmer, Phys. Chem. Miner. **30**, 353 (2003).
[15] K. J. Kingma, R. E. Cohen, R. J. Hemley, and H. K. Mao, Nature (London) **374**, 243 (1995).
[16] D. Andrault, G. Fiquet, F. Guyot, and M. Hanfland, Science **282**, 720 (1998).
[17] L. P. Huang and J. Kieffer, J. Chem. Phys. **118**, 1487 (2003).
[18] J. S. Tse and D. D. Klug, J. Chem. Phys. **95**, 9176 (1991).
[19] R. Guido, D. Valle, and H. C. Anderson, J. Chem. Phys. **94**, 5056 (1991).
[20] M. Wilson, P. A. Madden, M. Hemmati, and C. A. Angell, Phys. Rev. Lett. **77**, 4023 (1996).
[21] S. Tsuneyuki, M. Tsukada, A. Aoki, and Y. Matsui, Phys. Rev. Lett. **61**, 869 (1988).
[22] B. W. H. van Beest, G. J. Kramer, and R. A. van Santen, Phys. Rev. Lett. **64**, 1955 (1990).
[23] P. Tangney and S. Scandolo, J. Chem. Phys. **117**, 8898 (2002).
[24] D. Herzbach, K. Binder, and M. H. Muser, J. Chem. Phys. **123**, 124711 (2005).
[25] Y. F. Liang, C. R. Miranda, and S. Scandolo (unpublished).
[26] D. Herzbach and M. H. Muser, Comput. Phys. Commun. **174**, 17 (2006).
[27] L. V. Woodcock, C. A. Angell, and P. Cheeseman, J. Chem. Phys. **65**, 1565 (1976).
[28] P. Vashishta, R. K. Kalia, J. P. Rino, and I. Eppsjo, Phys. Rev. B **41**, 12197 (1990).
[29] K. J. Kingma and R. J. Hemley, Am. Mineral. **79**, 269 (1994).
[30] J. Etchepare, M. Merin, and L. Smetankine, J. Chem. Phys. **60**, 1873 (1974).
[31] P. F. McMillan and A. C. Hess, Phys. Chem. Miner. **17**, 97 (1990).
[32] F. Gervais and B. Pirious, Phys. Rev. B **11**, 3944 (1975).
[33] A. Rahmani, M. Benoit, and C. Benoit, Phys. Rev. B **68**, 184202 (2003).
[34] R. W. G. Wychoff, *Crystal Structures*, 2nd ed., (Krieger, Malabar, FL, 1982), Vol. 1 (one useful website is http://cst-www.nrl.navy.mil/lattice/).
[35] M. Ocana, V. Fornes, J. V. Garcia-Ramos, and C. J. Serna, Phys. Chem. Miner. **14**, 527 (1987).
[36] P. J. Heaney, Rev. Mineral. **29**, 1 (1994).
[37] P. Tangney and S. Scandolo, J. Chem. Phys. **119**, 9673 (2003).
[38] A. M. Hofmeister, J. Xu, and S. Akimoto, Am. Mineral. **75**, 951 (1990).
[39] L. P. Huang, M. Durandurdu, and J. Kieffer, e-print cond-mat/0602285.
[40] Handbook of Minerals Raman Spectra (http://www.ens-lyon.fr/LST/Raman).
[41] M. H. Muser and K. Binder, Phys. Chem. Miner. **28**, 746 (2001).
[42] M. G. Tucker, M. T. Dove, and D. A. Keen, J. Phys.: Condens. Matter **12**, L723 (2000).
[43] L. P. Huang and J. Kieffer, Phys. Rev. Lett. **95**, 215901 (2005).
[44] S. Tsuneyuki, H. Aoki, M. Tsukada, and Y. Matsui, Phys. Rev. Lett. **64**, 776 (1990).
[45] F. Liu, S. H. Garofalini, R. D. King-Smith, and D. Vanderbilt, Phys. Rev. Lett. **70**, 2750 (1993).
[46] I. P. Swainson and M. T. Dove, Phys. Rev. Lett. **71**, 193 (1993).
[47] M. B. Smirnov and A. P. Mirgorodsky, Phys. Rev. Lett. **78**, 2413 (1997).
[48] H. Kimizuka, H. Kaburaki, and Y. Kogure, Phys. Rev. Lett. **84**, 5548 (2000).
[49] R. J. Hemley, *High-Pressure Research in Mineral Physics*, edited by M. H. Manghani and Y. Syono (AGU, Washington, DC, 1987), pp. 347–359.
[50] R. J. Hemley, J. Shu, M. A. Carpenter, J. Hu, H. K. Mao, and K. J. Kingma, Solid State Commun. **114**, 527 (2000).
[51] B. B. Karki, M. C. Warren, L. Stirude, G. J. Ackland, and J. Crain, Phys. Rev. B **55**, 3465 (1997).
[52] C. Lee and X. Gonze, J. Phys.: Condens. Matter **7**, 3693 (1995); C. Lee and X. Gonze, Phys. Rev. B **56**, 7321 (1997).
[53] See, e.g., H. B. Yu and W. F. Van Gunsteren, Comput. Phys. Commun. **172**, 69 (2005).